Finite element simulation of direct deposition additive manufacturing for fiber reinforced thermoplastics

Zhaogui Wang[1], Zhenyu Fang[1], Douglas E. Smith[2]

[1]Department of Mechanical Engineering, Dalian Maritime University, Dalian, China, 116000
[2]Department of Mechanical Engineering, Baylor University, Waco, TX, USA, 76798

Abstract

Non-planar direct deposition additive manufacturing of polymer composites has recently seen increased attention from industries, where the molten plastics beads are extruded through a heated nozzle directly into three-dimensional space to form lightweight truss-like structures. This promising method shortens the manufacturing time and fabricates structures without stair-effect appearance that occurs in traditional layered additive manufacturing processes. This paper investigates the flow dynamics of fiber reinforced thermoplastics melt during a direct deposition process via a 2D planar deposition flow model. A quasi steady state for the deposition flow is assumed, where the flow-induced fiber orientation is evaluated through the Folgar-Tucker isotropic rotary diffusion model with the orthotropic-fitted closure approximation. The direct deposition process of a cubic lattice is simulated using finite element suite ABAQUS, where the orientation-homogenized material properties of a 13% CF-ABS are employed. Computed results indicate printing sequence affects the stress accumulation of the printed part notably.

Introduction

Polymer deposition Additive Manufacturing (AM) (otherwise known as fused filament fabrication or fused deposition modeling) is extending to large format manufacturing due to the implementation of efficient screw-extruder-based material feeding systems [1]. Due to the low-cost and high capability in building intricate structures, the large scale AM systems have seen continuously applications in automotive, aerospace and naval industries for rapid prototyping of large-dimension parts and tooling [2-5]. Due to the viscoelastic nature of the thermoplastic-based feedstock, molten polymers are able to be deposited freely in 3D space without support material underneath. This feature facilitates the rapid freeform fabrication of grid cells that exhibit lightweight feature yet high structural strength and stiffness. For instance, Branch Technology Inc. (Chattanooga, TN, USA) mounted a single screw extruder onto a robotic arm and deposited Carbon Fiber filled ABS (CF-ABS) polymers directly in open space forming the lattice structures as appearing in Figure 1 [6]. During the deposition process, the extruded bead rapidly transits from viscoelastic state to elastic state and thus provide sufficient stiffness for the cellular structure to be built upwards.

Carbon fiber filled thermoplastic composites provide additional stiffness and low thermal expansion that smooth the process of direct deposition additive manufacturing. In particular, the discontinuous fibers re-orient as the material flow being extruded and stretched in the process of direct deposition and thus the resulting fiber orientation in the beads affects the material properties of the manufactured grid cells. Nixon, et al. evaluated the internal geometric effects of the extrusion nozzle on the fiber orientation alignment using Moldflow software (Moldflow

Corporation, Framingham, MA, USA), where a convergent nozzle geometry was found to yield higher fiber alignment than a divergent designed nozzle [7]. Heller, et al. employed an axisymmetric 2D flow model via COMSOL (COMSOL Inc., Burlington, MA, USA) simulating the nozzle flow with a short section of free extrudate included, and found that the die swell at nozzle exit reduced the principal fiber orientation by ~20% [8]. Extended works based on Heller's model explored the non-Newtonian fluid rheology effects [9] and the screw swirling motion [10] on the resulting fiber orientation of an extrudate composite. Studies reviewed above are done following a weakly coupled formulation between the flow kinematics and fiber orientation evolution, such that the fibers' presence in the flow is ignored during the computation of the flow. A few studies performed fully coupled flow/orientation simulation for polymer deposition additive manufacturing, where depicted the mutually dependent interactions between the flow kinematics and fiber orientation kinetics (e.g., [11-13], while the fully coupled studies are mostly done for planar deposition flow. To reduce the complexity of the simulation, we start the flow modeling with the weakly coupled flow/orientation simulation, where the flow kinematics of a 2D Newtonian direction deposition (i.e., non-planar deposition) flow are solved firstly in ANSYS-Polyflow. Based on the solved flow kinematics, the fiber orientation state of the flow domain is then evaluated using the Advani-Tucker orientation tensor approach through the Folgar-Tucker fiber orientation evaluation equation with isotropic rotary diffusion and orthotropic fitted closure. Employing the solved fiber orientation tensors at flow end, the material properties of a deposited bead are estimated through the orientation homogenization method, including the elastic constants, coefficients of thermal expansion and thermal conductivity. Finally, the transient direct deposition process of a simple cubic lattice is simulated via ABAQUS with computed properties employed.

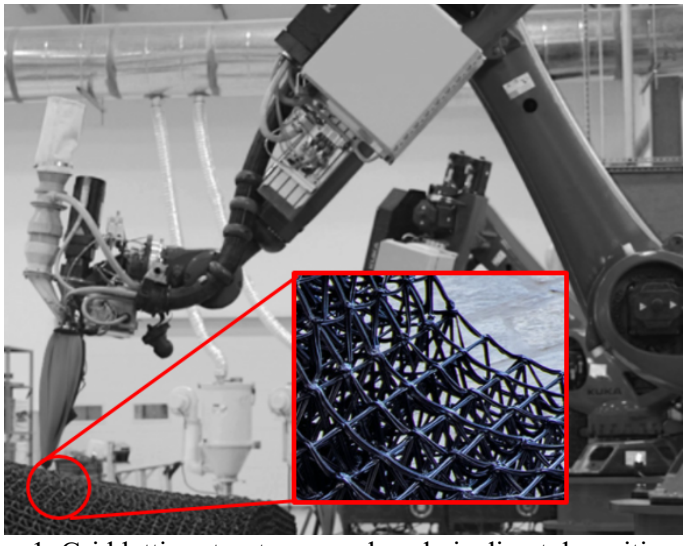

Figure 1. Grid lattice structures produced via direct deposition AM.

Governing Equations

Governing equations for numerical modeling of fiber reinforced composite material flow for direct deposition AM are introduced in this section, including the identifications of the material flow fields as well as the fiber orientation state within the direct deposition flow suspension.

Flow Fields Kinematics

An important component of direct deposition AM simulations is the identification of the composite melt flow fields in the extrusion nozzle, in which suspended fibers re-orientate due to the variation of the flow kinematics. Prior literatures [7-10] addressed the nozzle flow characterization through a decoupled formulation, where the flow fields are solved as if no fibers present in the polymer melt. An isothermal, incompressible, and highly viscous creeping flow is elsewhere considered in prior related work [8], where the thermal gradients, inertia effect, and the time transient effect are neglected. Under these assumptions, the mass the momentum conservation equations of the flow field can be, respectively, written as [14]

$$\nabla \cdot \boldsymbol{v} = 0, \tag{1}$$

and,

$$\nabla \cdot \boldsymbol{\sigma} + \rho \boldsymbol{f} = 0, \tag{2}$$

where $\boldsymbol{v}$ is the velocity tensor, ρ refers to the density of the continuum, $\boldsymbol{f}$ refers to the body force tensor, and $\boldsymbol{\sigma}$ is the Cauchy stress tensor, which can be written as [14]

$$\boldsymbol{\sigma} = 2\eta \boldsymbol{D} - \mathrm{P}\boldsymbol{I}, \tag{3}$$

where P is the pressure, $\boldsymbol{I}$ is the identity matrix, and η is the viscosity of Newtonian melt flow.

Specifically, this study simulates the transient process of a direct deposition flow and Polyflow solves the time-dependent flow such that [15]

$$\boldsymbol{M}(\boldsymbol{X})\dot{\boldsymbol{X}} + \boldsymbol{K}(\boldsymbol{X})\boldsymbol{X} + \boldsymbol{F}(\boldsymbol{X}) = 0 \tag{4}$$

which is subjected to the initial condition $\boldsymbol{X}(\mathrm{t}_0) = \boldsymbol{X}_0$. $\boldsymbol{X}$ is the vector of nodal unknowns such as velocity, and pressure in this study. $\dot{\boldsymbol{X}}$ is the time derivative of $\boldsymbol{X}$. $\boldsymbol{M}$ and $\boldsymbol{K}$ are the mass and stiffness matrices that are dependent on $\boldsymbol{X}$, and $\boldsymbol{F}$ vector corresponds to the volumetric forcing function and the natural boundary conditions [15].

Fiber Orientation Kinetics

Characterizing the fiber orientation kinetics for filled polymer systems in direct deposition AM applications is of great importance as the final alignment of fibers in the deposited materials significantly determines the strength, stiffness and warpage of a printed part. Jeffery's Equation [16] first expressed the motion of a single rigid ellipsoidal particle. Folgar and Tucker [17] extended Jeffery's theory to analyze the interactions between fibers in a non-dilute fiber suspension. Further, Advani and Tucker [18] defined the fiber orientation tensor approach to quantify the fiber alignment state for concentrated suspension systems, which requires fewer independent variables than that of the Folgar-Tucker model[17]. The Advani-Tucker equation can be written as [18]

$$\frac{D\boldsymbol{A}}{Dt} = (\boldsymbol{W}\cdot\boldsymbol{A} - \boldsymbol{A}\cdot\boldsymbol{W}) + \lambda(\boldsymbol{D}\cdot\boldsymbol{A} + \boldsymbol{A}\cdot\boldsymbol{D} - 2\mathbb{A}{:}\boldsymbol{D}) + 2\,C_I\dot{\gamma}(\boldsymbol{I} - 3\boldsymbol{A}), \tag{5}$$

where the second and fourth-order fiber orientation tensors are defined respectively as

$$\boldsymbol{A} = <\boldsymbol{pp}>, \text{ and } \mathbb{A} = <\boldsymbol{pppp}>, \tag{6}$$

Here, $\boldsymbol{p}$ is the unit vector depicting the orientation of a single rigid fiber along the axis of fiber alignment. The angle bracket "< >" refers to an average over all directions, weighted by the probability distribution function of the orientation [12]. λ is a factor counting the geometric effects of the fibers reinforced. For an ellipsoidal fiber, λ can be evaluated as [18]

$$\lambda = \frac{(a_r)^2 - 1}{(a_r)^2 + 1}, \tag{7}$$

where a_r is the hydrodynamic aspect ratio of the ellipsoidal fiber. C_I is an empirical coefficient that including the fiber-fiber interactions. Bay proposed an expression of C_I as [19],

$$C_I = 0.0184\exp(-0.7148 v_f a_r), \tag{8}$$

where v_f refers to the fiber volume fraction of the composite system. In addition, $\boldsymbol{W}$ and $\boldsymbol{D}$ are the vorticity tensor and rate-of-deformation tensor of the suspension flow, respectively, which can be written as

$$\boldsymbol{D} = (\nabla \boldsymbol{v} + \nabla \boldsymbol{v}^T)/2 \text{ and } \boldsymbol{W} = (\nabla \boldsymbol{v} - \nabla \boldsymbol{v}^T)/2, \tag{9}$$

where $\nabla \boldsymbol{v}$ indicates the flow gradient field and the superscript T refers to the matrix transpose operation.

Direct Deposition Flow Modelling

Heller, et al. [8] (see also [9,10]) reported that the internal geometry of the nozzle has a notable impact on the fiber orientation of the extruded composite, since the flow domain geometry defined by the interior of the nozzle determines the melt flow velocity gradient fields. To this end, we consider the nozzle melt flow simplified as a 2D planar model, including the flow inside the nozzle and a short strand of free extrudate, as appearing in Figure 2. The dimension of the nozzle flow is based on the geometrical design of a Strangpresse large-scale additive manufacturing Model 19 single screw extruder nozzle, as given in [9]. The initial distance between the nozzle end and material substrate is 3 mm, as a common layer thickness employed in large scale AM applications [13]. The boundary conditions of the flow domain labeled in Figure 2, such that

- Flow inlet, where a fully developed velocity profile is imposed. The velocity profile is computed based on the prescribed volumetric flow rate of $3.05 \times 10^{-4}\ m^3/s$, which corresponds to a mass flow rate at about approximately 9 lb/hour for 13% CF-ABS, which is a typical material feed rate in large scale AM extruders [13].
- No-slip wall, where $v_t = v_n = 0$, and v_t and v_n refer to the tangential and normal velocity of a node.
- Free surface, where $\boldsymbol{v} \cdot \boldsymbol{n} = 0$, and $\boldsymbol{v}$ and $\boldsymbol{n}$ donate the velocity vector and normal vector of a node.
- Extrudate-substrate contact surface, where geometries contact detection (algorithm provided in Polyflow) is set.
- Material substrate, where v_n = -0.106 m/s is imposed to simulate the relative motion between the nozzle and the substrate, which equals to the averaged vertical velocity of the flow at the nozzle exit, also see [13])

The hyperbolic form of Equation 5 requires an initial condition of the second-order fiber orientation tensor at the flow inlet. Herein, we imposed a fully developed fiber orientation state reported by Heller, et al. [8], assuming that the orientation state reaches somewhat a steady state at the inlet of the flow. The flow domain is meshed with 4-node quadrilateral element, and a total of 3508 elements with 3719 nodes, which is proved as a sufficient and efficient mesh quality through a mesh sensitivity study.

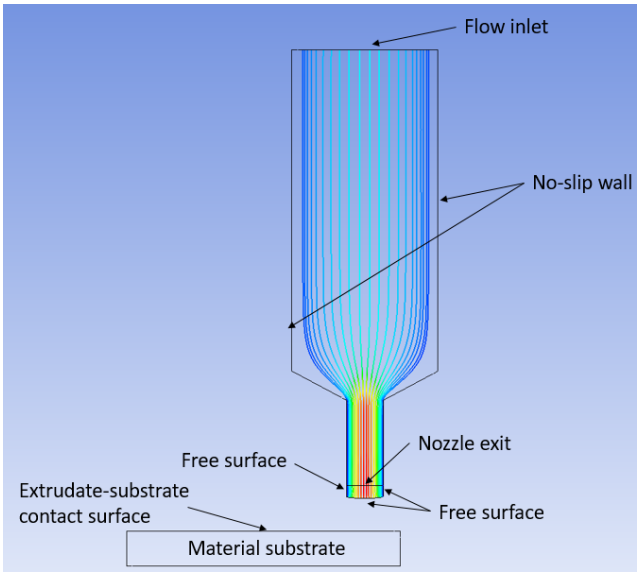

Figure 2. Boundaries of the flow domain of interest.

The transient velocity kinematics along flow streamlines are plotted through Figures 3-6 with a time increment of 0.05 second, in which the velocity variations during the deposition process can be viewed. It is seen that the flow end exhibits a similar velocity contour as long as the direct material deposition speed equals to the nozzle vertically-moving speed. Therefore, we assume a quasi-steady state of the fiber orientation could be achieved at the end of the flow.

Further, the second order fiber orientation tensors are evaluated along the streamline data of simulation at t = 0.2 second (cf. Figure 6), where the quasi-steady state of fiber orientation is assumed to be achieved at the flow end of the domain (i.e., contact surface between flow end and substrate). In the fiber orientation computation, the fiber aspect ratio is assumed as 15, in an averaged sense, which is a safe estimation based on prior studies on similar composite materials (e.g., [20,21]). The C_I is set as 0.01, as did in a similar study [10]. The orientation tensors diagonal components are given in Figures 7-9 (cf. flow streamlines locations are shown in Figure 10). It is seen that the fibers re-orientate intensely as being extruded out of the nozzle (i.e., at locations where horizontal coordinates of Figures 7 to 9 are around zero) and quickly recovers to a stable status as directly deposited onto the substrate (i.e., horizontal coordinates proceed to -0.02), which implies that the fibers could reach a steady state at the flow end.

The fiber orientation tensors diagonal components at flow end across the radial direction of the nozzle is given in Figure 11, which is then employed in the orientation homogenization approach [18] to predict the material properties of solidified deposited composites. The carbon fiber and ABS matrix properties are given in Table 1, and the computed properties of 13 wt.% CF-ABS (i.e., volume fraction is about 8.4%) are given in Table 2 sequentially. The computed properties appearing in Table 2 will be employed in the macro-level direct deposition AM process simulation shown in next section.

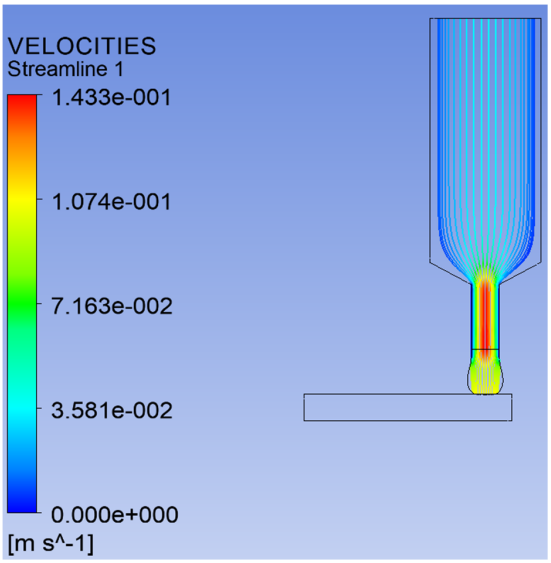

Figure 3. Direct deposition flow at t= 0.05 second.

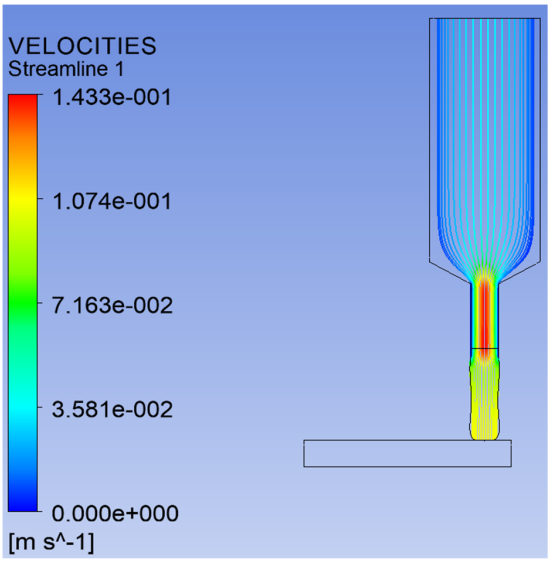

Figure 4. Direct deposition flow at t= 0.10 second.

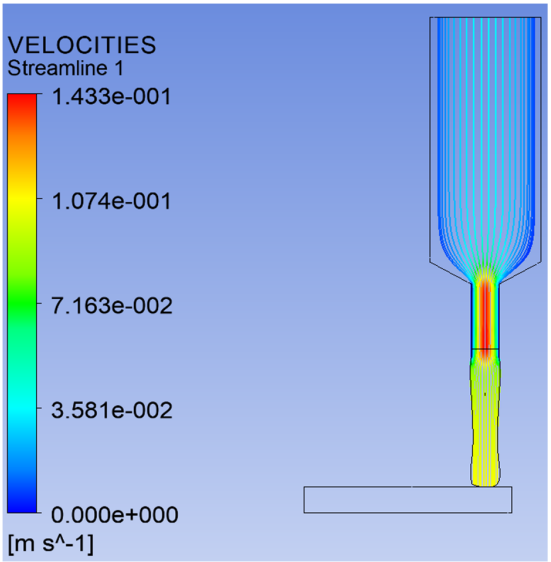

Figure 5. Direct deposition flow at t= 0.15 second.

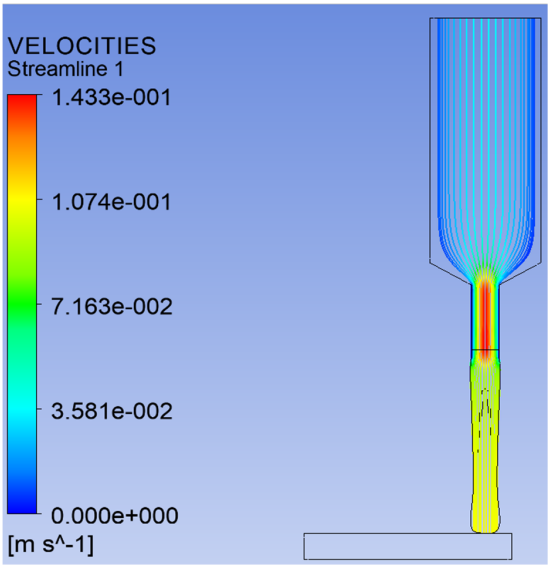

Figure 6. Direct deposition flow at t= 0.20 second.

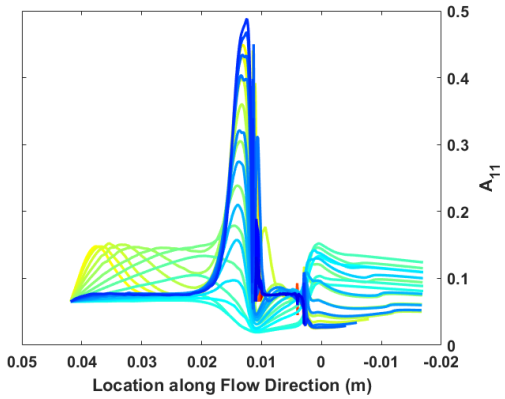

Figure 7. Fiber orientation tensor component A_{11} along flow direction.

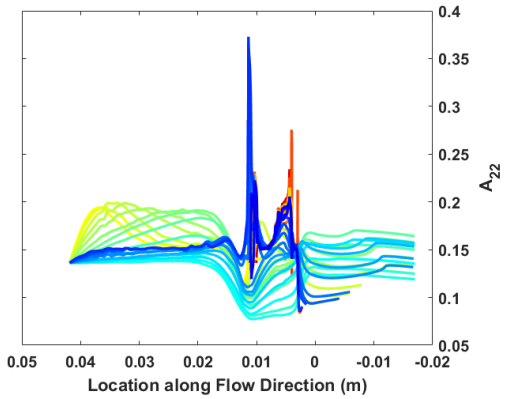

Figure 8. Fiber orientation tensor component A_{22} along flow direction.

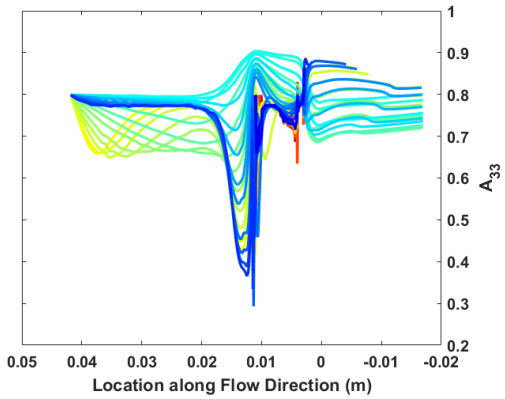

Figure 9. Fiber orientation tensor component A_{33} along flow direction.

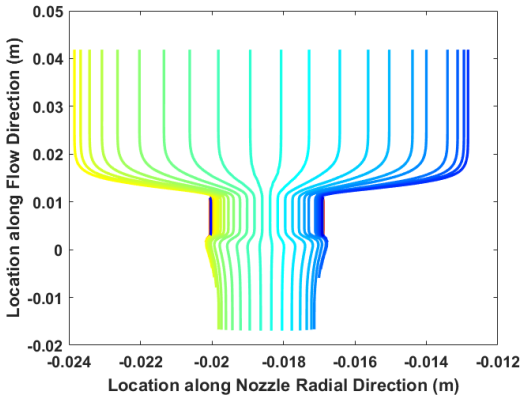

Figure 10. Flow streamlines locations for direction deposition flow.

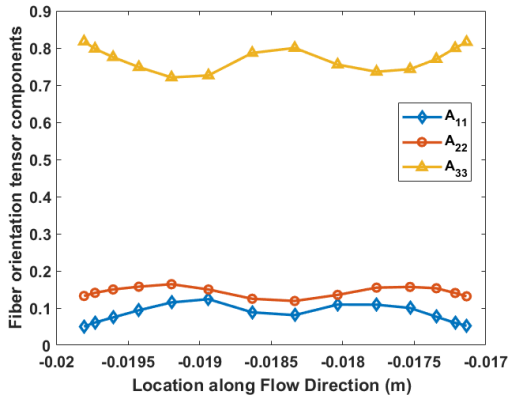

Figure 11. Fiber orientation across a direct deposited bead.

Table 1. Material properties of the phase materials of a 13% CF-ABS.

Material	E (GPa)	G (GPa)	ν	CTE	κ $(\frac{W}{m \cdot K})$
ABS matrix	2.25	0.83	0.35	90e-6	0.175
Carbon fiber	230	96	0.2	-0.6e-6	3.06

Table 2. Material properties of a 13% CF-ABS estimated by orientation homogenization.

Direction	E (GPa)	G (GPa)	ν	CTE	κ $(\frac{W}{m \cdot K})$
11	8.28	N/A	N/A	25.38e-6	0.463
22	3.45	N/A	N/A	69.84e-6	0.163
33	3.21	N/A	N/A	81.40e-6	0.135
12	N/A	1.52	0.37	N/A	N/A
13	N/A	1.30	0.38	N/A	N/A
23	N/A	1.14	0.44	N/A	N/A

Finite Element Simulation of Cubic Lattice Cell Direction Deposition

Employing computed thermal-mechanical properties of 13% CF-ABS, we simulate the transient thermal-mechanical history for direction deposition AM of a simple cubic lattice via finite element suite, ABAQUS, via the built-in element activation/deactivation function. The printing process is divided into an element-by-element activation process, where the stem time for activating each element is 0.1 second. The boundary conditions are set as appearing in Figure 12, where the substrate and ambient temperatures are 40 ℃ and the heat convection coefficient is 82 $W/(m^2\ K)$, adopting from [22]. Specifically, it is important to note that the deposited material exhibits a high degree of material anisotropy, as appearing in Table 2. In direct deposition AM, the principal direction of the beads' anisotropy (maximum magnitude of the properties among the Cartesian coordinates directions) is determined by the direction of deposition. To this end, we employ different material orientation local coordinates based on the material loading direction, as seen in Figure 12 (i.e., coordinates 11-22-33). Besides, the dimensions of a unit deposition element is 3 mm in thickness, 8 mm in width, 8 mm in length, representing a 3 mm nozzle depositing beads with a moving speed at 80 mm/s. The dimension of the printed cubic cell is 40mm*40mm*24mm.

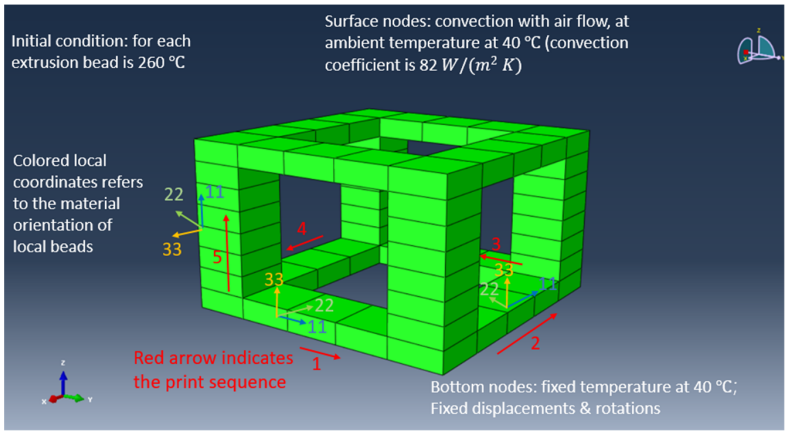

Figure 12. Finite element simulation setup for a simple cubic lattice direct deposition process.

The temperature field of the printed cell is shown in Figures 13 and 14, where the conditions in as-printed state and cooled down state are given, respectively. Herein, the cooling time is set as 300 second as large-dimension extruded beads require longer time to reach the ambient temperature. The fixed displacements boundary conditions applied on the bottom nodes are not removed during the cooling post-processing, indicating that the cubic cell is cooled without being taken away from the printing substrate. The substrate and convection ambient temperatures are set as 40 °C assuming the printing is performed inside a temperature-controlled furnace. In Figure 13, it can be seen that the temperature decreases slowly during the printing process due in part to the large-dimension of a single extrusion unit. This brings up an issue where the vertically deposited polymers remaining in relatively high temperatures are still in semi-molten status and may not be able to provide enough stiffness to support the upper deposited beads. Herein, we note that a further study on printing/cooling balance is needed to ensure these vertically deposited beads are reduced below Tg temperature before the next planar beads are deposited. Nevertheless, we expect that the vertically deposited beads could support the upper planar deposited beads as the overall print size is still limited in small scale. After cooled down by 300 seconds, the overall cubic cell roughly reaches the ambient temperature, as seen in Figure 14. The bottom beads exhibit lower temperature than the upper beads (i.e., no support underneath) as the heat conduction between the ABS composite and material substrate is more efficient in heat exchanging as compare to the heat convection between the extruded beads and the air flow. Additionally, the vertically deposited beads are in relatively higher temperature among the entire printed domain.

Furthermore, we plot the Mises stress fields and the deformation fields in Figures 15 and 16 and Figures 17 and 18, respectively. And the results are also given in as-printed and cooled-down conditions. During the printing process (cf. Figure 15), the maximum stress occurs at the bottom beads that contacting the substrate, in which the beads are restricted by the substrate and thus thermal residual stress accumulates. This is similar to a traditional layered manufacturing process. Nevertheless, the maximum stresses are seen in the vertically deposited beads in the cooled down condition (cf. Figure 16), and the magnitude of the maximum stress increases two orders as compared to that in as-printed condition. In addition, from the contours shown in Figures 17 and 18, it is seen that the maximum deformation occurs in the upper beads of the cubic cell, and increases one order of magnitude after being cooled down. The unique stress concentration and maximum deformation implies that the optimization of thermal post-processing is necessary to reduce the potential defects in the direct deposited lattice structures, which is expected to be explored by our presented simulation approach in other in-depth studies.

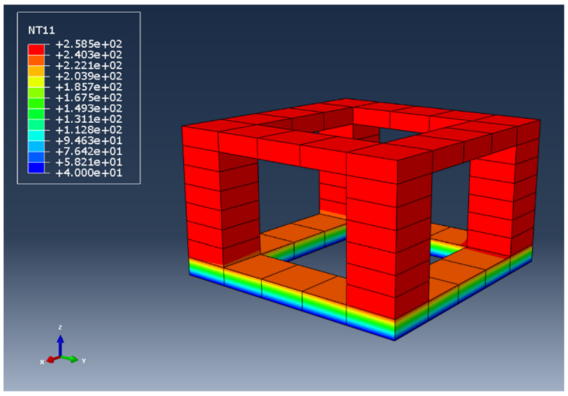

Figure 13. Temperature field of the as-printed cell.

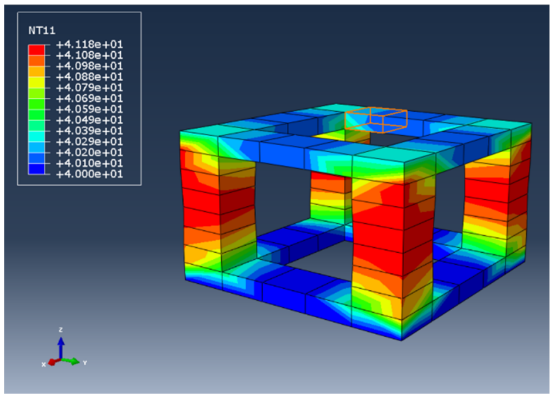

Figure 14. Temperature field of the cooled-down cell.

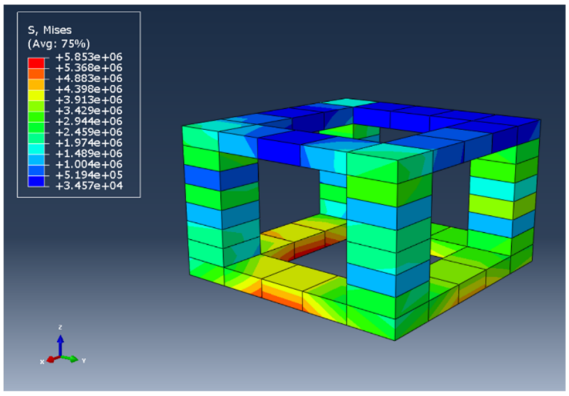

Figure 15. Mises stress field of the as-printed cell.

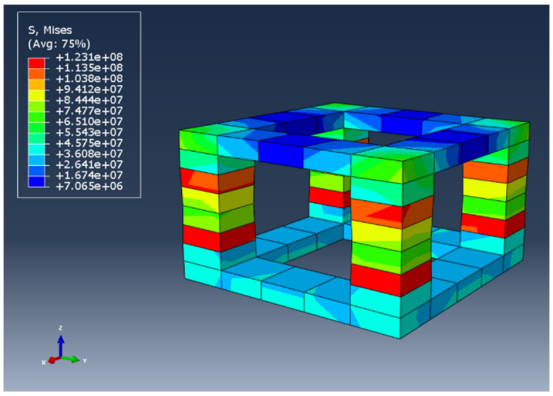

Figure 16. Mises stress field of the cooled-down cell.

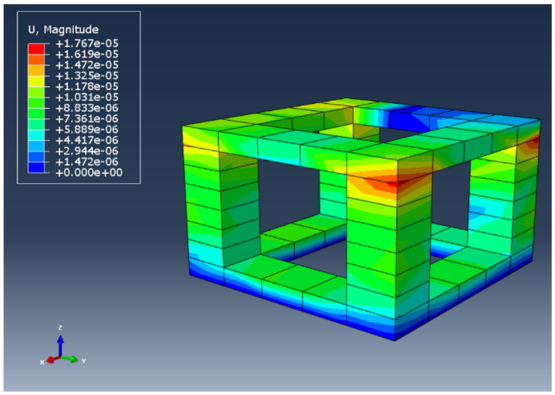

Figure 17. Deformation field of the as-printed cell.

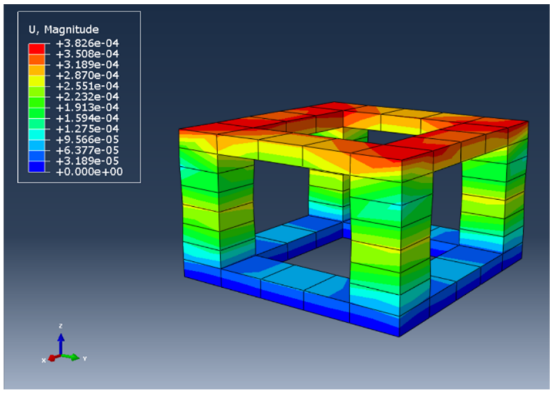

Figure 18. Deformation field of the cooled-down cell.

Conclusion

A two-step numerical study is performed to simulate the direct deposition AM process. The weakly coupled flow/orientation analysis is adopted for a direction deposition AM nozzle flow. The transient extrusion deposition flow kinematics are solved by ANSYS Polyflow, where a quasi-steady state is assumed to be achieved at the end of the transient simulation. The Advani-Tucker approach is employed to evaluate the second order orientation tensors along streamlines of the modelled flow. Evaluated orientation tensors at the flow end are adopted to the orientation-homogenization-based properties evaluation to estimate the material properties of the 13% CF-ABS material extrudates. Direct deposition AM of a simple cubic cell is simulated by using the ABAQUS suite, where the transient thermal-mechanical history of the printed part is computed. The results indicated that the direct deposition is a promising AM approach for freeform fabrication of lightweight lattice grid-cells, while the printing/cooling timing balance is needed to ensure enough stiffness for upper deposited beads can be provided from vertically deposited beads. In addition, larger value of residual stresses is seen in vertically deposited beads as compared to planar deposited beads. To this end, we suggest to optimized post-cooling processing to reduce the thermal stress and deformation occurrences.

Acknowledgements

The authors would like to thank Dalian Maritime University and Baylor University for the support on this project. This work was supported by the Fundamental Research Funds for the Central Universities of China (No. 3132021337).

References

[1] Love, Lonnie J., et al. "The importance of carbon fiber to polymer additive manufacturing." Journal of Materials Research 29. 17 (2014): 1893-1898.
[2] Talagani M R, DorMohammadi S, Dutton R, et al. Numerical simulation of big area additive manufacturing (3D printing) of a full size car. Sampe Journal, 2015, 51(4): 27-36.
[3] Nieto D M, López V C, Molina S I. Large-format polymeric pellet-based additive manufacturing for the naval industry. Additive Manufacturing, 2018, 23: 79-85.
[4] Peterson E. Technical Challenges to Adopting Large Scale Additive Manufacturing for the Production of Yacht Hulls. International Conference on Human Systems Engineering and Design: Future Trends and Applications. Springer, Cham, 2020: 15-20.
[5] Post B K, Chesser P C, Lind R F, et al. Feasibility of using Big Area Additive Manufacturing to Directly Manufacture Boat Molds. Oak Ridge National Lab.(ORNL), Oak Ridge, TN (United States), 2018.
[6] Branch Technology. https://www.branch.technology/ (accessed on 07.06.2021).
[7] J. Nixon, B. Dryer, D. Chiu, I. Lempert, and D. I. Bigio, “Three parameter analysis of fiber orientation in fused deposition modeling geometries,” Annu. Tech. Conf. - ANTEC Conf. Proc., vol. 2, pp. 985–995, Jan. 2014.
[8] Heller B P, Smith D E, Jack D A. Effects of extrudate swell and nozzle geometry on fiber orientation in Fused Filament Fabrication nozzle flow. Additive Manufacturing, 2016, 12: 252-264.
[9] Wang Z, Smith D E. Rheology effects on predicted fiber orientation and elastic properties in large scale polymer composite additive manufacturing. Journal of Composites Science, 2018, 2(1): 10.
[10] Wang Z, Smith D E. Numerical analysis of screw swirling effects on fiber orientation in large area additive manufacturing polymer composite deposition. Composites Part B: Engineering, 2019, 177: 107284.
[11] Bertevas E, Férec J, Khoo B C, et al. Smoothed particle hydrodynamics (SPH) modeling of fiber orientation in a 3D printing process. Physics of Fluids, 2018, 30(10): 103103.
[12] Wang Z, Smith D E. Finite element modelling of fully-coupled flow/fiber-orientation effects in polymer composite deposition additive manufacturing nozzle-extrudate flow. Composites Part B: Engineering, 2021, 219: 108811.
[13] Wang Z, Smith D E. A Fully Coupled Simulation of Planar Deposition Flow and Fiber Orientation in Polymer Composites Additive Manufacturing. Materials, 2021, 14(10): 2596.
[14] Baird D G, Collias D I. Polymer processing: principles and design. John Wiley & Sons, 2014.
[15] ANSYS, Inc, “ANSYS Polyflow user's guide Release 15.0.”.
[16] G.B. Jeffery. The motion of ellipsoidal particles immersed in a viscous fluid. Proc. R. Soc. London, Ser. A, 102 (715) (1922), pp. 161-179.
[17] F. Folgar, C.L. Tucker III. Orientation behavior of fibers in concentrated suspensions. J. Reinf. Plast. Compos., 3 (2) (1984), pp. 98-119.
[18] S.G. Advani, C.L. Tucker III. The use of tensors to describe and predict fiber orientation in short fiber composites. J. Rheol., 31 (8) (1987), pp. 751-784.
[19] 54. Bay, R.S. Fiber Orientation in Injection-Molded Composites: A Comparison of Theory and Experiment. Ph.D. Thesis, Univer-sity of Illinois at Urbana-Champaign, Champaign, IL, USA, 1991.
[20] Ning F, Cong W, Qiu J, et al. Additive manufacturing of carbon fiber reinforced thermoplastic composites using fused deposition modeling. Composites Part B: Engineering, 2015, 80: 369-378.

[21] Wang Z, Smith D E, Jack D A. A statistical homogenization approach for incorporating fiber aspect ratio distribution in large area polymer composite deposition additive manufacturing property predictions. Additive Manufacturing, 2021, 43: 102006.
[22] Zhang Y, Chou Y K. Three-dimensional finite element analysis simulations of the fused deposition modelling process. Proceedings of the Institution of Mechanical Engineers, Part B: Journal of Engineering Manufacture, 2006, 220(10): 1663-1671.